International Journal of Rotating Machinery
2001, Vol. 7, No. 2, pp. 143–151
Reprints available directly from the publisher
Photocopying permitted by license only

Stability Analysis of a Gear Pair System Supported by Squeeze-Film Dampers

T.N. SHIAU[a,*], J.R. CHANG[b] and S.T. CHOI[b]

[a]*Department of Mechanical Engineering, National Chung Cheng University, 621 Chia Yi, Taiwan;*
[b]*Institute of Aeronautics and Astronautics, National Cheng Kung University, 701 Tainan, Taiwan*

(Received 24 April 1998; In final form 12 November 1999)

This paper examines the stability of the steady-state periodic response of a gear pair system supported by squeeze-film dampers. The steady-state response of the system is obtained by using the hybrid technique of Harmonic Balance Method and Time Collocation. The Floquet–Liapunov theory is used to perform the stability analysis of the first variation equations with periodic coefficients, which is generated by the perturbation technique. The stability charts on gear mesh stiffness, spin ratio, disk unbalance, gravity, and squeeze-film damper are used to perform parameter studies. The numerical results show that the unstable region always occurs when the spin ratio is near the second coupled mode of the gear pair system. Furthermore, the mesh stiffness has a significant influence on the coupled critical speeds. Therefore, it plays an important role in determining the spin ratio stability range.

Keywords: Stability analysis, Gear pair system, Squeeze-film damper, Hybrid method, Floquet–Liapunov theory

INTRODUCTION

Gear rotor-bearing systems are one of the most common mechanisms for modern power transmission. On account of the ever increasing demand for power and high speed transportation, research in the field of geared rotor dynamics has become very important. The dynamic analysis of a geared rotor-bearing system is an essential step in the development of high performance machinery.

Rao *et al.* (1995) included the effect of pressure angle, developed a finite element model for determining the coupled bending-torsion natural frequencies and mode shape of geared rotor. Squeeze-film dampers are now commonly used to suppress the lateral vibrations due to rotor unbalance. Mohan and Hahn (1974) considered the design of squeeze-film damper supports for rigid rotors. Cookson and Kossa (1979) considered the effectiveness of squeeze-film dampers for rigid rotors without a centralizing spring. Hwang and Shiau (1991) developed a Generalized Polynomial Expansion method to study the nonlinear effects of squeeze-film forces on flexible rotors. They applied the Harmonic Balance Method (HBM) and the Collocation Method to determine the system

* Corresponding author. Tel.: 886-5-2720411-6105. Fax: 886-5-2720589. E-mail: imetls@ccunix.ccu.edu.tw.

response. Shiau and Hwang (1993) studied the stability of a nonlinear rotor supported by squeeze-film dampers by using Floquet–Liapunov theory. Chen *et al.* (1993) considered the application of squeeze-film dampers to control lateral vibrations of a gear pair system. They reported one result using a Poincaré section from Direct Integration Method which indicated chaos in the system. Shiau *et al.* (1999) considered coupled bending-torsion vibrations of a gear pair due to unbalance and gravity. Considering the nonlinear squeeze-film damper forces, the route to chaos was established by using bifurcation maps. In geared rotor systems, it was also shown that torsional excitation can induce lateral vibrations and squeeze-film dampers can suppress large amplitudes of whirl due to the torsional excitation.

In this paper, a gear pair system supported by squeeze-film dampers with six degrees of freedom is considered. The hybrid technique, which combines the merits of the HBM and Time Collocation (TC), is employed to determine the steady-state periodic response due to unbalance and gravity. With the perturbation technique, the first variation equations with periodic coefficients are generated. The Floquet–Liapunov theory is used to examine the system stability. The stability charts based on the parameters of mesh stiffness, spin ratio, disk unbalance, gravity effect, and squeeze-film damper force are plotted.

GOVERNING EQUATION

A simple gear pair, Rao *et al.* (1995), mounted on squeeze-film damper supports is considered. The nonlinear squeeze-film damper, unbalance, and gravity force are the excitations on the system. The model of the squeeze-film damper is based on short bearing theory with the assumption of a fully cavitated oil film. The equations of motion can be expressed as

$$[M]\{\ddot{q}\} + (c_h[S_h] + [C])\{\dot{q}\} + (k_h[S_h] + [K])\{q\} = \{Q\} + \{F_d\} \tag{1}$$

where

$$[S_h] = \begin{bmatrix} s^2 & sc & r_1 s & -s^2 & -sc & r_2 s \\ sc & c^2 & r_1 c & -sc & -c^2 & r_2 c \\ r_1 s & r_1 c & r_1^2 & -r_1 s & -r_1 c & r_1 r_2 \\ -s^2 & -sc & -r_1 s & s^2 & sc & -r_2 s \\ -sc & -c^2 & -r_1 c & sc & c^2 & -r_2 c \\ r_2 c & r_2 c & r_1 r_2 & -r_2 s & -r_2 c & r_2^2 \end{bmatrix}$$

$$\{Q\} = \begin{Bmatrix} M_1 e_1 \Omega_1^2 \cos(\Omega_1 t + \Psi_1) \\ M_1 e_1 \Omega_1^2 \sin(\Omega_1 t + \Psi_1) - M_1 g \\ 0 \\ M_2 e_2 \Omega_2^2 \cos(\Omega_2 t + \Psi_2) \\ M_2 e_2 \Omega_2^2 \sin(\Omega_2 t + \Psi_2) - M_2 g \\ 0 \end{Bmatrix}, \tag{2}$$

$$\{F_d\} = \begin{Bmatrix} Fv_1 \\ Fw_1 \\ 0 \\ Fv_2 \\ Fw_2 \\ 0 \end{Bmatrix}$$

$$\{q\}^T = [V_1 \; W_1 \; \alpha_1 \; V_2 \; W_2 \; \alpha_2]$$

and the non-zero elements of $[M]$, $[C]$, and $[K]$ are

$$\begin{aligned} &M_{11} = M_{22} = M_1, \quad M_{44} = M_{55} = M_2, \\ &\quad M_{33} = I_{P1}, \quad M_{66} = I_{P2}, \\ &C_{11} = C_{22} = C_1, \quad C_{44} = C_{55} = C_2, \\ &K_{11} = K_{22} = K_1, \quad K_{44} = K_{55} = K_2 \end{aligned} \tag{3}$$

The matrices $[M]$ and $[C]$ denote the mass matrix and the damping matrix, respectively. The matrix $[K]$ is stiffness matrix associated with the centering spring. The gear mesh matrix is denoted as $[S_h]$. The

vector {Q} is a linear force vector composed of the excitation of unbalance and gravity. The vector $\{F_d\}$ denotes the nonlinear squeeze-film damper forces.

The nonlinear squeeze-film damper forces $\{F_d\}$ in radial and tangential direction based on short bearing theory, Mohan and Hahn (1974), are given by

$$F_r = -\frac{\mu R L^3}{C_r^2}(\varepsilon\dot{\phi}A_{11} + \dot{\varepsilon}A_{02})$$
$$F_\phi = -\frac{\mu R L^3}{C_r^2}(\varepsilon\dot{\phi}A_{20} + \dot{\varepsilon}A_{11}) \tag{4}$$

with

$$A_{ij} = \int_{\phi_g+\pi}^{\phi_g+2\pi} \frac{\sin^i\theta\cos^j\theta}{(1-\varepsilon\cos\theta)^3}\,\mathrm{d}\theta$$
$$\phi_g = \tan^{-1}\frac{\dot{\varepsilon}}{-\varepsilon\dot{\phi}} \tag{5}$$

The above forces can also be expressed in the horizontal and vertical directions in the following form:

$$F_V = (F_r V - F_\phi W)/\sqrt{V^2+W^2}$$
$$F_W = (F_r W + F_\phi V)/\sqrt{V^2+W^2} \tag{6}$$

A non-dimensional form of Eq. (1) is

$$[I]\{\bar{q}''\} + \left(\frac{2\zeta_h}{\Omega_r}[\bar{S}_h] + \frac{2\zeta}{\Omega_r}[\bar{C}]\right)\{\bar{q}'\}$$
$$+ \left(\frac{\xi_K}{\Omega_r^2}[\bar{S}_h] + \frac{1}{\Omega_r^2}[\bar{K}]\right)\{\bar{q}\} = \{\bar{Q}\} + \{\bar{F}_d\} \tag{7}$$

where $[I]$ is the identity matrix,

$$[\bar{S}_h] = \begin{bmatrix} s^2 & sc & \frac{s}{\xi_c} & -s^2 & -sc & \frac{\eta_r s}{\xi_c} \\ sc & c^2 & \frac{c}{\xi_c} & -sc & -c^2 & \frac{\eta_r c}{\xi_c} \\ \xi_I\xi_c s & \xi_I\xi_c c & \xi_I & -\xi_I\xi_c s & -\xi_I\xi_c c & \xi_I\eta_r \\ -\frac{s^2}{\eta_M} & -\frac{sc}{\eta_M} & -\frac{s}{\eta_M\xi_c} & \frac{s^2}{\eta_M} & \frac{sc}{\eta_M} & -\frac{\eta_r s}{\eta_M\xi_c} \\ -\frac{sc}{\eta_M} & -\frac{c^2}{\eta_M} & -\frac{c}{\eta_M\xi_c} & \frac{sc}{\eta_M} & \frac{c^2}{\eta_M} & -\frac{\eta_r c}{\eta_M\xi_c} \\ \frac{\xi_I\xi_c\eta_r s}{\eta_I} & \frac{\xi_I\xi_c\eta_r c}{\eta_I} & \frac{\xi_I\eta_r}{\eta_I} & -\frac{\xi_I\xi_c\eta_r s}{\eta_I} & -\frac{\xi_I\xi_c\eta_r c}{\eta_I} & \frac{\xi_I\eta_r}{\eta_I} \end{bmatrix} \quad \{\bar{Q}\} = \begin{Bmatrix} U_1\cos(\tau+\Psi_1) \\ U_1\sin(\tau+\Psi_1) - \frac{W_g}{\Omega_r^2} \\ 0 \\ \frac{U_2}{\eta_r^2}\cos\left(-\frac{\tau}{\eta_r}+\Psi_2\right) \\ \frac{U_2}{\eta_r^2}\sin\left(-\frac{\tau}{\eta_r}+\Psi_2\right) - \frac{W_g}{\Omega_r^2} \\ 0 \end{Bmatrix},$$

$$\{\bar{F}_d\} = \begin{Bmatrix} \frac{S_D}{\Omega_r}f_{v1} \\ \frac{S_D}{\Omega_r}f_{w1} \\ 0 \\ \frac{S_D}{\eta_M\Omega_r}f_{v2} \\ \frac{S_D}{\eta_M\Omega_r}f_{w2} \\ 0 \end{Bmatrix} \quad f_v = \frac{(f_r v - f_\phi w)}{\sqrt{v^2+w^2}} \quad f_w = \frac{(f_r w + f_\phi v)}{\sqrt{v^2+w^2}} \quad f_r = -(\varepsilon\phi' A_{11} + \varepsilon' A_{02}) \quad f_\phi = -(\varepsilon\phi' A_{20} + \varepsilon' A_{11})$$

$$\{\bar{q}\}^T = [v_1 \quad w_1 \quad \alpha_1 \quad v_2 \quad w_2 \quad \alpha_2] = \left[\frac{V_1}{C_r} \quad \frac{W_1}{C_r} \quad \alpha_1 \quad \frac{V_2}{C_r} \quad \frac{W_2}{C_r} \quad \alpha_2\right] \tag{8}$$

and the non-zero elements of $[\bar{C}]$ and $[\bar{K}]$ are

$$\begin{aligned} \bar{C}_{11} &= \bar{C}_{22} = 1, \quad \bar{C}_{44} = \bar{C}_{55} = \frac{\eta_C}{\eta_M}, \\ \bar{K}_{11} &= \bar{K}_{22} = 1, \quad \bar{K}_{44} = \bar{K}_{55} = \frac{\eta_K}{\eta_M} \end{aligned} \tag{9}$$

The symbols used in the above equations are $\eta_M = M_2/M_1$, $\eta_I = I_{P2}/I_{P1}$, $\eta_r = r_2/r_1$, $\eta_C = C_2/C_1$, $\eta_K = K_2/K_1$, $\xi_c = C_r/r_1$, $\xi_I = M_1 r_1^2/I_{P1}$, $\xi_K = k_h/K_1$, $\zeta = C_1/(2M_1\omega_1)$, $\zeta_h = C_h/(2M_1\omega_1)$, $\omega_1 = \sqrt{K_1/M_1}$, $\Omega_r = \Omega_1/\omega_1$, $\tau = \Omega_1 t$, $S_D = (\mu R L^3)/(M_1 C_r^3 \omega_1)$, $U = e/C_r$, $W_g = g/C_r\omega_1^2$, and $' = \mathrm{d}/\mathrm{d}\tau$.

STABILITY ANALYSIS

A hybrid method, Hwang and Shiau (1991), which combines the merits of both the HBM and TC is employed to obtain the steady-state response of Eq. (7). To investigate the stability of steady-state periodic solution $\{\bar{q}\}_{ss}$, a perturbation technique is used. Let the response $\{\bar{q}\}$ be expressed in the form as

$$\{\bar{q}\} = \{\bar{q}\}_{ss} + \{\delta\bar{q}\} \tag{10}$$

where $\{\delta\bar{q}\}$ represents a perturbation of the original steady-state response. The stability will depend on perturbation response $\{\delta\bar{q}\}$.

Substituting Eq. (10) into Eq. (7) and knowing that $\{\bar{q}\}_{ss}$ satisfies Eq. (7), the equations of motion governing the perturbation response can be expressed as

$$\begin{aligned} &[I]\{\delta\bar{q}''\} + \left(\frac{2\zeta_h}{\Omega_r}[\bar{S}_h] + \frac{2\zeta}{\Omega_r}[\bar{C}]\right)\{\delta\bar{q}'\} \\ &\quad + \left(\frac{\xi_K}{\Omega_r^2}[\bar{S}_h] + \frac{1}{\Omega_r^2}[\bar{K}]\right)\{\delta\bar{q}\} \\ &\quad = \{\bar{F}_d(\{\bar{q}\}, \{\bar{q}'\}, \tau)\} - \{\bar{F}_d(\{\bar{q}\}_{ss}, \{\bar{q}'_{ss}\}, \tau)\} \end{aligned} \tag{11}$$

With the Taylor series expansion in the first order approximation, the right-hand side of Eq. (11) can be approximated as

$$\begin{aligned} &\{\bar{F}_d(\{\bar{q}\}, \{\bar{q}'\}, \tau)\} - \{\bar{F}_d(\{\bar{q}\}_{ss}, \{\bar{q}'_{ss}, \tau)\} \\ &\quad = [A_1(\tau)]\{\delta\bar{q}\} + [A_2(\tau)]\{\delta\bar{q}'\} \end{aligned} \tag{12}$$

where the matrices $[A_1(\tau)]$ and $[A_2(\tau)]$ are defined by

$$\begin{aligned} [A_1(\tau)] &= \left.\frac{\partial\{\bar{F}_d\}}{\partial\{\bar{q}\}}\right|_{\{\bar{q}\}=\{\bar{q}\}_{ss}} \\ [A_2(\tau)] &= \left.\frac{\partial\{\bar{F}_d\}}{\partial\{\bar{q}'\}}\right|_{\{\bar{q}\}=\{\bar{q}\}_{ss}} \end{aligned} \tag{13}$$

Substitution of Eq. (13) into Eq. (11) with rearrangement yields first variational equations as

$$[I]\{\delta\bar{q}''\} + [\boldsymbol{C}]\{\delta\bar{q}'\} + [\boldsymbol{K}]\{\delta\bar{q}\} = \{0\} \tag{14}$$

where

$$\begin{aligned} [\boldsymbol{C}] &= \left(\frac{2\zeta_h}{\Omega_r}[\bar{S}_h] + \frac{2\zeta}{\Omega_r}[\bar{C}] - [A_2(\tau)]\right) \\ [\boldsymbol{K}] &= \left(\frac{\varepsilon_K}{\Omega_r^2}[\bar{S}_h] + \frac{1}{\Omega_r^2}[\bar{K}] - [A_1(\tau)]\right) \end{aligned} \tag{15}$$

The stability of the nonlinear steady-state response is governed by Eq. (14) which is a set of homogeneous ordinary differential equations. Since the coefficient matrices in the system equations are periodic functions of time, the stability of the system can be examined using Floquet–Liapunov theory, Shiau and Hwang (1993). The transition matrix of the periodic system is established and its eigenvalues are extracted. The stability criterion states that the system is stable only if the maximum absolute eigenvalue of the transition matrix is smaller than one. This can be expressed as

$$\begin{aligned} |\Lambda|_{max} &< 1.0 : \text{Stable} \\ |\Lambda|_{max} &\geq 1.0 : \text{Unstable} \end{aligned} \tag{16}$$

NUMERICAL EXAMPLES

A six degree of freedom gear pair system supported by centralized squeeze-film dampers, Fig. 1, is taken

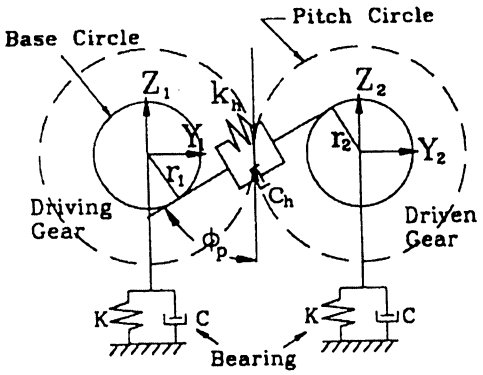

FIGURE 1 A gear-pair bearing system.

TABLE I Non-dimensional parameters of the gear pair system

ξ_I	2	ξ_C	10^{-5}
ξ_K	1	η_M	1
η_C	1	η_K	1
η_r	1	η_I	1
ζ_h	0.01	ζ	0.01
S_D	0.1	W_g	0.5
U_1	0.1	U_2	0.1
Ω_r	variables	ϕ_P	22.5°
Ψ_1	0°	Ψ_2	0°

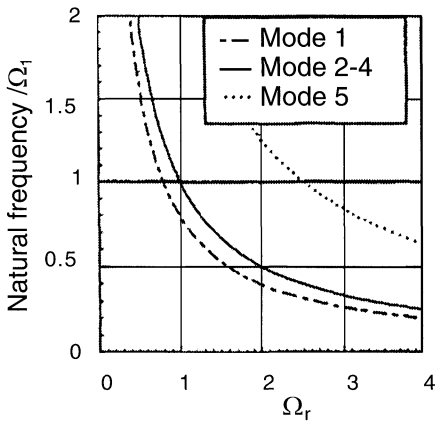

FIGURE 2 Natural frequency diagram.

as a sample configuration to investigate the effect of nonlinear dynamic behaviors. The non-dimensional parameters of the system are listed in Table I and the natural frequency diagram is shown in Fig. 2. It shows that the critical speeds due to synchronous excitation occur at Ω_r equal to 0 (rigid body torsional), 0.792 (coupled), 1.0 (three lateral), 2.524 (coupled).

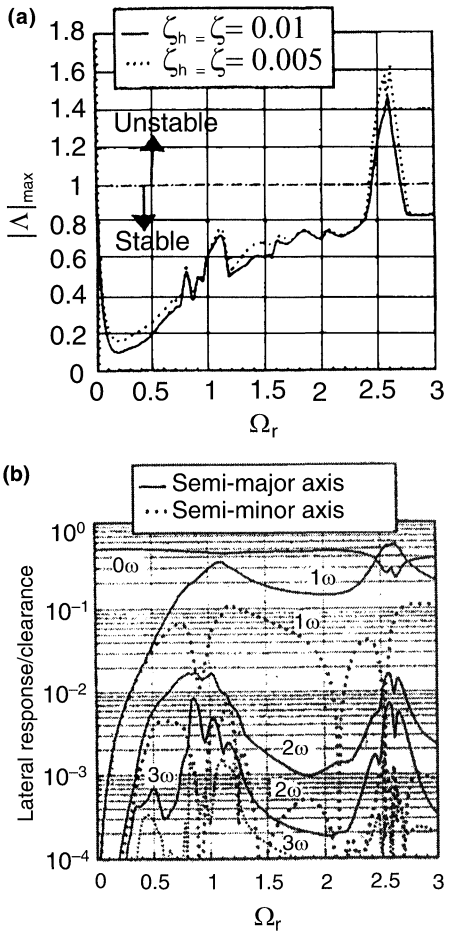

FIGURE 3 (a) Maximum absolute eigenvalues $|\Lambda|_{max}$ for $U_1 = U_2 = 0.1$, $W_g = 0.5$, $S_D = 0.1$, $\xi_K = 1$. (b) Lateral response of driving gear for $U_1 = U_2 = 0.1$, $W_g = 0.5$, $S_D = 0.1$, $\xi_K = 1$.

The steady-state periodic response is obtained by using the hybrid method (HBM + TC). The stability of the periodic responses is obtained using Floquet theory. Figure 3(a) shows the maximum absolute value, $|\Lambda|_{max}$, of the eigenvalues of transition matrix for two different damping ratios, 0.01 and 0.005. The unstable zone shown in Fig. 3(a) occurs in the range of $\Omega_r = 2.46$–2.71 for the case, $\zeta_h = \zeta = 0.01$, and that of $\Omega_r = 2.43$–2.74 for the case, $\zeta_h = \zeta = 0.005$. For light damping, the unstable region is a little wider. The unstable zone for both cases is around the second coupled mode.

The first three harmonic components of both the non-dimensional semi-major and semi-minor axes, 1ω, 2ω, and 3ω, associated with a constant offset, 0ω, versus spin ratio are plotted to illustrate the steady-state periodic responses of the driving gear for $\zeta_h = \zeta = 0.01$ as shown in Fig. 3(b). The higher harmonic components of response are found very small compared with the first harmonic component of response. It is seen that the semi-major axis amplitude of the first harmonic component is larger than the constant offset only when the Ω_r is near the unstable region which is around the second coupled mode.

The orbital response of the driving gear at $\Omega_r = 1.0$, using the hybrid method, is shown in Fig. 4(a) and by using the Newmark method with two different initial conditions is also shown in Fig. 4(b) and (c). Two initial conditions (I, II) are considered. Initial condition I is zero initial condition. The initial lateral responses and velocities of value 0.6 and the initial torsional responses and velocities of value 6×10^{-6} are considered for initial condition II. As shown in Fig. 3(a), the system periodic response at $\Omega_r = 1.0$ is stable, and the steady-state orbits shown in Fig. 4(a)–(c) approach the same limit cycle. When the system is operating at $\Omega_r = 2.6$, the steady-state periodic response obtained by using the hybrid method is unstable as was shown in Fig. 3(a). The motion orbit of the driving gear at $\Omega_r = 2.6$ is shown in Fig. 5(a)–(d). The orbit shown in Fig. 5(a) is obtained by using the hybrid method and thus used in the stability analysis. Figure 5(b) and (c) show the transient motion of the driving gear calculated by the numerical integration method with different initial conditions, I and II, for the first 40 consecutive rotations. The orbits obtained with two different initial conditions approach the same steady-state response, which is also shown in Fig. 5(d). However it is quite different from that by using the hybrid method as shown in Fig. 5(a). To classify the orbit of Fig. 5(d), the FFT semi-major axis spectrum corresponding to the time history and the associated Poincaré map are also shown in Fig. 5(e) and (f), respectively. It is seen that the stable steady-state response of Fig. 5(d), obtained by using Newmark's method, is essentially quasi-periodic, Shiau *et al.* (1999).

Further analysis of the parameter influence on the stability is studied. It is difficult to determine the unstable zones from the above figures. Therefore, stability charts are made to show the instability zones for different parameter combinations. From these charts it is much easier to see the influence of a certain parameter on the stability. The number of plots can also be reduced since two variables can be shown in the same chart.

The parameters of the gear pair system given in Table I and $W_g = 0.3$ are used. The stability chart in Fig. 6 shows the influence of unbalance and spin ratio with the unbalance values ranging from 0.05 to 0.2, and Ω_r from 0 to 3. Two major unstable zones are found, one is near the lateral mode and the other is around the second coupled mode. The unstable zone for the left one and the right one occurs when the unbalance values U_1 and U_2 are

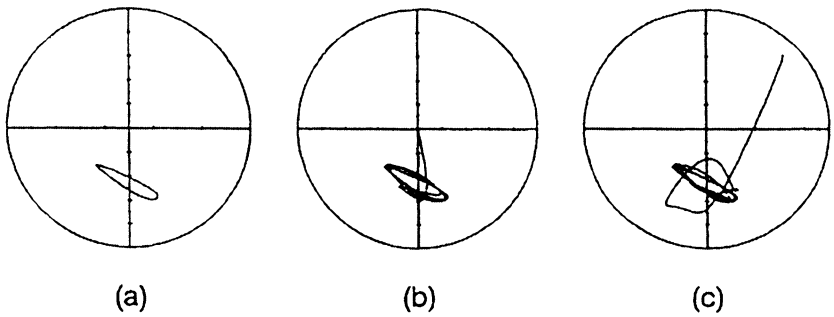

FIGURE 4 Driving gear (a) orbit by hybrid method (HBM + TC), (b) orbit by Newmark method with initial condition I, (c) orbit by Newmark method with initial condition II for $\Omega_r = 1$, $U_1 = U_2 = 0.1$, $W_g = 0.5$, $S_D = 0.1$, $\xi_K = 1$.

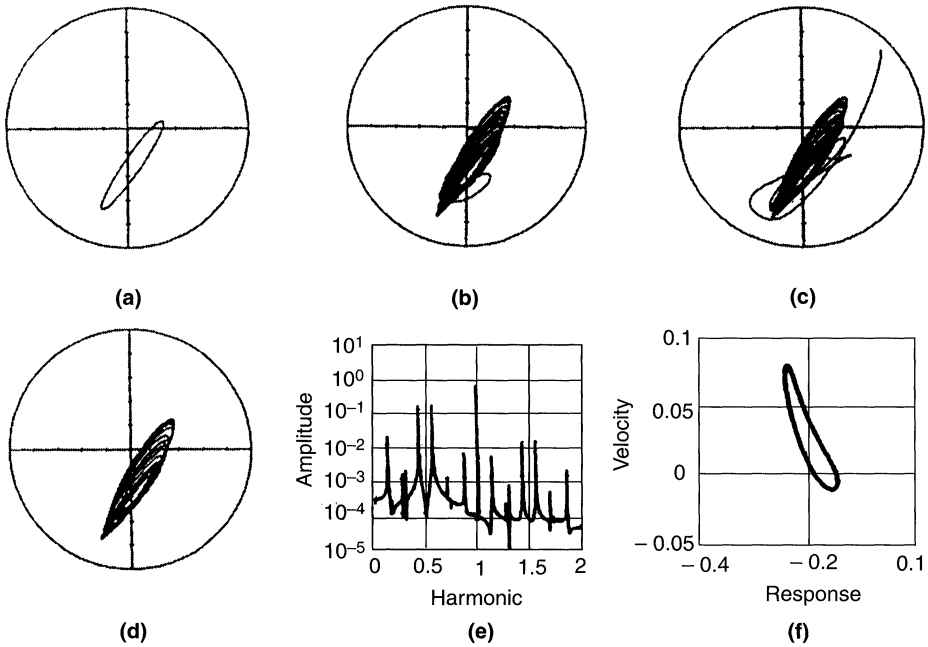

FIGURE 5 Driving gear (a) orbit by hybrid method (HBM + TC), (b) orbit by Newmark method with initial condition I, (c) orbit by Newmark method with initial condition II, (d) orbit by Newmark method (steady-state response), (e) spectrum of semi-major axis response, (f) Poincaré map for horizontal response for $\Omega_r = 2.6$, $U_1 = U_2 = 0.1$, $W_g = 0.5$, $S_D = 0.1$, $\xi_K = 1$.

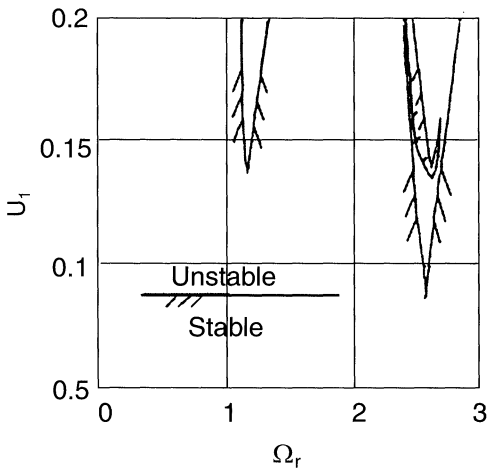

FIGURE 6 Stability chart on $U_1 = U_2$ and Ω_r for $W_g = 0.3$, $S_D = 0.1$, $\xi_K = 1$.

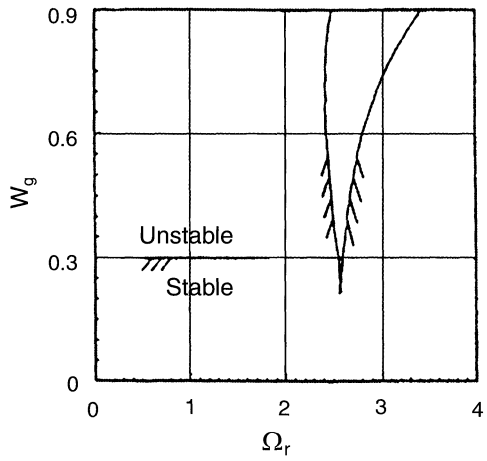

FIGURE 7 Stability chart on W_g and Ω_r for $U_1 = U_2 = 0.1$, $S_D = 0.1$, $\xi_K = 1$.

larger than 0.137, and 0.087, respectively. It is also seen that the interior of the unstable zone around the second coupled mode has a narrow stable region.

In Fig. 7 the gravity effect has been studied. The solution becomes unstable in the interval from $\Omega_r = 2.46$–2.71 at $W_g = 0.5$ of Fig. 7. This is the same as that of Fig. 3(a). It also shows that the

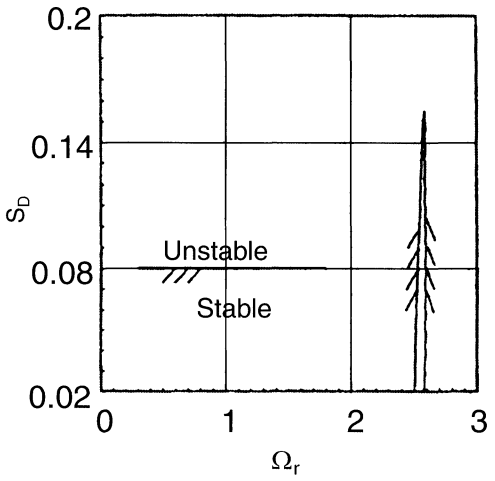

FIGURE 8 Stability chart on S_D and Ω_r for $U_1 = U_2 = 0.1$, $W_g = 0.3$, $\xi_K = 1$.

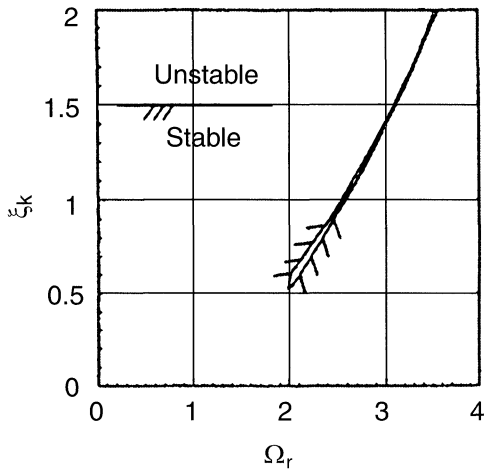

FIGURE 9 Stability chart on ξ_K and Ω_r for $U_1 = U_2 = 0.1$, $W_g = 0.3$, $S_D = 0.1$.

instability zone only occurs around the second coupled mode and the unstable range of Ω_r gets wider if gravity W_g increases. If the gravity is smaller than 0.215, the solution is stable regardless of the value of Ω_r.

The stability chart for investigating the influence of squeeze-film damping is shown in Fig. 8. In this chart, only one unstable zone is found around the second coupled mode and it is stable when the value of S_D is larger than 0.155. For smaller values of S_D, the unstable range of Ω_r increases.

Figure 9 shows a stability chart for the variables of mesh stiffness ratio, ξ_K, and spin ratio, Ω_r. It is clear that the value of Ω_r near which an unstable zone occurs is quite different from the previous stability charts and is very sensitive to the value of ξ_K. An explanation may be that the range of Ω_r at which the unstable zone occurs is near the second coupled mode. It can be verified from the critical speeds for different value of ξ_K as given in Table II. From Table II, e.g. $\xi_K = 2$, the critical speeds are 0.80 (coupled), 1.0 (three lateral), and 3.51 (coupled) and from Fig. 9 it is shown that the unstable region for $\xi_K = 2$ ranges from $\Omega_r = 3.54$–3.58. This is very near the second coupled mode, $\Omega_r = 3.51$.

TABLE II Critical speeds for different ξ_K

Mode no.	$\xi_K = 0.5$	$\xi_K = 1.0$	$\xi_K = 1.5$	$\xi_K = 2.0$
1(C)	0.77	0.79	0.80	0.80
2(L)	1.0	1.0	1.0	1.0
3(L)	1.0	1.0	1.0	1.0
4(L)	1.0	1.0	1.0	1.0
5(C)	1.85	2.52	3.06	3.51

CONCLUSIONS

A stability analysis is performed by using the hybrid method to obtain the steady-state periodic response and then solving the eigenvalues of the Floquet transition matrix for the perturbed response. When the solutions are stable, the steady-state orbits obtained by using the Newmark method and the hybrid method are in good agreement. From the stability charts, it may be concluded that the unstable region always occurs when the value of the spin ratio is near the second coupled mode. Furthermore, the mesh stiffness has a significant influence on the coupled critical speeds. Therefore, it strongly influences the spin ratio at which the system is stable.

Acknowledgment

The authors wish to thank Professor J.S. Rao from Indian Institute of Technology, New Delhi, for his valuable suggestions.

NOMENCLATURE

$[C]$	damping matrix
C	damping coefficient of bearing
c	$\cos\phi_{\mathrm{P}}$
c_{h}	damping coefficient of gear mesh
e	eccentricity of disk
$\{F_{\mathrm{d}}\}$	forcing vector due to squeeze-film dampers
$[I]$	identity matrix
I_{P}	polar mass moment of inertia of disk
$[K]$	stiffness matrix
k_{h}	stiffness coefficient of gear mesh
K	stiffness coefficient of bearing
$[M]$	mass matrix
M	mass of disk
$\{Q\}$	force vector due to unbalance and gravity
$\{q\}$	displacement vector
R, C_{r}, L	radius, radial clearance, and width, respectively, of squeeze-film damper
r	radius of base circle of gear
$[S_{\mathrm{h}}]$	gear mesh matrix
S_{D}	non-dimensional coefficient of squeeze-film damper force; $\mu RL^3/(M_1 C_{\mathrm{r}}^3 \omega_1)$
s	$\sin\phi_{\mathrm{P}}$
U	non-dimensional eccentricity; e/C_{r}
(V, W)	lateral displacements in (Y, Z) directions
W_g	non-dimensional gravity force; $g/(C_{\mathrm{r}}\omega_1^2)$
α	torsion angle about X axis
ε	non-dimensional radial displacement of journal center
$\zeta, \zeta_{\mathrm{h}}$	$C_1/(2M_1\omega_1)$, and $C_{\mathrm{h}}/(2M_1\omega_1)$, respectively
η_M, η_C, η_K	(M_2/M_1), (C_2/C_1), and (K_2/K_1), respectively
η_I, η_r	(I_{P2}/I_{P1}), and (r_2/r_1), respectively
$\lvert\Lambda\rvert_{\max}$	maximum absolute eigenvalue of transition matrix
μ	viscosity of lubricant
ξ_c, ξ_I, ξ_K	(C_{r}/r_1), $(M_1 r_1^2/I_{P1})$, and (k_{h}/K_1), respectively
ϕ	precession angle of journal center
ϕ_{P}	pressure angle of gear pair
Ψ	phase angle of disk unbalance
Ω	rotating speed
Ω_{r}	spin ratio; (Ω_1/ω_1)
ω_1	$\sqrt{K_1/M_1}$
τ	non-dimensional time; $\Omega_1 t$

Subscript

d, h	squeeze-film damper and gear mesh, respectively
r, ϕ	radial and tangential direction, respectively
V, W	horizontal and vertical direction, respectively
1, 2	first and second gear or bearing, respectively

References

Chen, C.S., Natsiavas, S. and Nelson, H.D. (1993) Coupled lateral-torsional vibration of a gear pair system supported by squeeze-film damper, *Nonlinear Vibration ASME, Design Engineering Division* DE V.54, New York, p. 53.

Cookson, R.A. and Kossa, S.S. (1979) The effectiveness of squeeze-film damper bearings supporting rigid rotors without a centralizing spring, *Int. J. Mech. Sci.*, **21**, 639.

Hwang, J.L. and Shiau, T.N. (1991) An application of the generalized polynomial expansion method to nonlinear rotor bearing systems, *J. Vib. Acous., ASME*, **113**, 299.

Mohan, S. and Hahn, E.J. (1974) Design of squeeze-film damper supports for rigid rotors, *Journal of Engineering for Industry*, 976.

Rao, J.S., Chang, J.R. and Shiau, T.N. (1995) Coupled bending-torsion vibration of geared rotors, *ASME Design Engineering Technical Conferences*, DE-Vol. 84-2, Vol. 3 – Part B, p. 977.

Shiau, T.N. and Hwang, J.L. (1993) Generalized polynomial expansion method for the dynamic analysis of rotor-bearing systems, *Journal of Engineering for Gas turbines and Power, Trans ASME*, **115**, 209.

Shiau, T.N., Rao, J.S., Chang, J.R. and Choi, S.T. (1999) Dynamic behavior of geared rotors, *Journal of Engineering for Gas turbines and Power, Trans ASME*, **121**, 494–503.